

Soft Matter

Accepted Manuscript



This is an *Accepted Manuscript*, which has been through the Royal Society of Chemistry peer review process and has been accepted for publication.

Accepted Manuscripts are published online shortly after acceptance, before technical editing, formatting and proof reading. Using this free service, authors can make their results available to the community, in citable form, before we publish the edited article. We will replace this *Accepted Manuscript* with the edited and formatted *Advance Article* as soon as it is available.

You can find more information about *Accepted Manuscripts* in the [Information for Authors](#).

Please note that technical editing may introduce minor changes to the text and/or graphics, which may alter content. The journal's standard [Terms & Conditions](#) and the [Ethical guidelines](#) still apply. In no event shall the Royal Society of Chemistry be held responsible for any errors or omissions in this *Accepted Manuscript* or any consequences arising from the use of any information it contains.

Foams stabilised by mixtures of nanoparticles and oppositely charged surfactants: Relationship between bubble shrinkage and foam coarsening

Armando Maestro,^{1,†,*} Emmanuelle Rio,¹ Wiebke Drenckhan,¹ Dominique
Langevin¹ and Anniina Salonen,¹

¹*Laboratoire de Physique des Solides, Bâtiment 510, Université Paris-Sud XI,
91405-Orsay (France)*

[†]*Present Address: Cavendish Laboratory, University of Cambridge, JJ Thompson
Avenue, CB3 0EH Cambridge, UK*

**E-mail: am2212@cam.ac.uk*

Soft Matter Accepted Manuscript

Abstract

We have studied foams stabilised by surfactant-decorated nanoparticles adsorbed at the bubble surfaces. We show that the controlled compression of a single bubble allows to understand the coarsening behavior of these foams. When bubbles are compressed, the particles become tightly packed in the surface layer. They lose their mobility, and the interface becomes solid-like when the jammed state is reached. Further compression leads to interfacial buckling characterised by crumpled surfaces. We find that the surface concentration of particles at which the jamming and the buckling transitions occur are independent of the surfactant concentration. This is a surprising feature. It suggests that the surfactants are mandatory to help the particles adsorb at the interface and that they change the equilibrium surface concentration of the decorated particles. But they do not affect the surface properties once the particles are adsorbed. We measured the compression elastic modulus of the surface in the jammed state and found it to be compatible with the Gibbs condition for which the spontaneous dissolution of bubbles is arrested. Due to this effect, the coarsening process of a foam composed of many close-packed bubbles occurs in two steps. In the first step, coarsening is slow and coalescence of the bigger bubbles is observed. In the second step, a number of very small bubbles remains, which exhibit crumpled surfaces and are stable over long times. This suggests that foam coarsening is arrested once the smallest bubbles become fully covered after the initial shrinking step.

1. Introduction

Liquid foams are dispersions of gas bubbles in a continuous liquid phase, and are metastable systems¹. Their unstable nature is a critical issue in a variety of well-established industrial applications – ranging from food and cosmetics to oil-recovery and phase-selective catalysis².

Most of the time, foams are stabilised using surface active agents such as surfactants adsorbed at the bubble surface³. In addition to the decrease in surface tension γ , the surface layer gives rise to a resistance to compression, characterised by a surface elastic compression modulus E . Recently, colloidal particles have been used to create bubbles⁴⁻⁶ or foams which are stable for months or years⁷⁻¹³. This increasing bubble lifetime is due to the ability of the surface layers formed by suitably chosen particles to prevent (or, at least, slow down) both film rupture (coalescence) and gas diffusion between bubbles (coarsening or Ostwald ripening). The detailed mechanisms of the stabilisation of foams against coarsening by particles are still under debate. In a collection of bubbles, gas transfer from smaller to larger bubbles –due to differences in Laplace pressure– leads to a compression of the interfaces of the shrinking bubbles. If the particles do not desorb during compression, the elastic surface modulus E will eventually increase. When the particles are sufficiently highly packed, the bubble surface can become solid-like, and further compression may induce surface buckling as observed on single bubbles¹⁴. When this happens, numerical simulations have shown that Ostwald ripening of an ensemble of spherical bubbles can be arrested if $E > \gamma/2$ ¹⁵. This was suggested earlier by Gibbs considering the behavior of a single bubble¹⁶ and was confirmed by experiments on foams stabilised by particles⁸ and proteins¹⁷.

Recent studies of the compression of oil droplets covered by particles (or polymers) evidenced the onset of a jamming transition beyond which the drop surface becomes

solid, followed by a buckling transition after which the drops become non-spherical¹⁸⁻²⁰. Similar observations have been made at flat oil-water and¹⁸ air-water surfaces²⁰⁻²³. The key condition in order to observe such behaviour is to avoid particle desorption during compression²⁴. The affinity of the colloidal particles for the gas/liquid interface is therefore crucial²⁵. This affinity depends on the wetting behaviour of the particles which is given by the balance between the solid-liquid, liquid-gas, and gas-solid interfacial tensions, and which is quantified by the contact angle θ . As a result, when θ is around 90° and when the particle is not too small, the energy of desorption largely exceeds the thermal energy kT (k being the Boltzmann constant, T the absolute temperature), and the adsorption becomes irreversible.

Although particles with chemically modified surfaces can be used⁷, an easier and more versatile approach to modify the wettability of the particles is the *in-situ* adsorption of amphiphilic molecules onto the particle surface²⁶⁻²⁸. The surface free energy for their attachment to a gas/liquid interface can be adjusted by changing the surfactant concentration, and surfactant-decorated nanoparticles can irreversibly adsorb at the air-water surface^{29, 30}. This prompted us to study the interfacial properties of these systems, in relation with foam properties.

Dispersions of colloidal silica particles mixed with an oppositely charged surfactant, hexadecyl trimethyl ammonium bromide (CTAB) were extensively studied by Ravera et al²⁹⁻³¹. They have demonstrated that the electrostatic interaction between the negatively charged surface of the particles and the positively charged surfactants promotes the adsorption of the surfactant onto the particle surface which increases its hydrophobicity, and thus transfers the particles from the bulk to the interface.

In the present work, we chose to focus on this system, since is very promising to stabilise foams because of the irreversible adsorption of the particles at the interface. In

particular we correlate the interfacial mechanical properties of the system with the ageing of the foams it stabilizes. We thus present an investigation of systems stabilised by such colloidal silica-CTAB dispersions. We determined the elastic response of the particle-laden gas/water interfaces on single interfaces and individual bubbles. In particular, we used a deflating bubble method to apply a mechanical solicitation similar to the one experienced by a bubble during coarsening and to measure the elastic modulus E in conditions similar to the ones occurring during coarsening^{18, 32}. The mechanical properties of the interfaces were studied for a range of surfactant concentrations, which results in different particle contact angles. In parallel we investigated the time evolution and stability of foams made with the same dispersions. Our main goal was to determine if the compression behaviour of the surface layers of individual bubbles can lead to the arrest of foam coarsening.

2. Materials and Methods

2.1. Chemicals

We used a commercial aqueous colloidal dispersion containing 34 wt.% of spherical silica nanoparticles *Ludox TMA* (Sigma). The particles have a diameter of 15 ± 2 nm, a specific surface area of $140 \text{ m}^2/\text{g}$ and a density ρ of $2.1 \text{ g}/\text{cm}^3$. The dispersion has a pH close to 6-7 due to the negatively charged nanoparticles. The cationic surfactant, hexadecyltrimethylammonium bromide, CTAB ($M_w = 346.46 \text{ g}/\text{mol}$), was also purchased from Sigma, with a purity $\geq 99\%$, and used without further purification. Water was double distilled and deionised by a MilliQ-RG system from Millipore, with a resistivity higher than $18 \text{ M}\Omega \cdot \text{cm}^{-1}$. In line with previous experiments^{33, 34}, salt was added (1mM NaBr) to the surfactant solutions, to promote adsorption. The NaBr (Sigma-Aldrich) was roasted at 600°C for 24 h before use in order to eliminate surface

active impurities. The absence of residual contamination was checked by measuring the surface tension of pure water containing 1 mM NaBr at 20°C which gave $\gamma = 72.5 \pm 0.2$ mN/m.

In order to avoid particle aggregation during the preparation of the dispersions, the original Ludox TMA dispersion was diluted to 1 wt.% by adding the surfactant solution drop-by-drop while applying a continuous stirring, following the procedure reported by Ravera et al²⁹. At the highest concentrations of CTAB some bulk aggregation of the particles was visible, but the aggregate size remained small as no sediment was seen.

2.2. Methods

a) Studies of individual bubbles (Rising bubble technique)

The adsorption of surfactant-decorated colloids from the aqueous dispersions to the air/water surface is monitored by measuring the surface tension γ . We use a commercial tensiometer Tracker instrument (Teclis, France) in the rising bubble configuration (a bubble immersed in water) and measure the surface tension as a function of time, keeping the volume constant. The surface tension –with a resolution ± 0.1 mN/m– is calculated by image analysis from the shape of the bubble. The shape depends on the balance between the surface tension and the density difference between the fluids and is described using the well-known Laplace equation³⁵. We define γ_0 as the equilibrium value of the surface tension at the end of the adsorption process. Once equilibrium is reached, the bubble is compressed at a rate of 0.5 mL/s. During the compression, the surface tension γ is measured as a function of the bubble radius R . This method allows the determination of the surface compression modulus E using

$$E = A \frac{d\gamma}{dA} = \frac{R}{2} \frac{d\gamma}{dR}. \quad (1)$$

We are also able to measure the pressure difference between the inside and the outside of the rising bubble as a function of time by a differential pressure sensor incorporated into the Tracker instrument.

All the experiments carried out in this work have been conducted at room temperature ($20\pm 1^\circ\text{C}$).

b) Foaming and foam stability

The foams were made by hand-shaking 3 ml of aqueous dispersions of the CTAB decorated particles contained in a glass bottle. Visual observations of foams by a digital camera (Ueye) were combined with microscopic observations of the bubbles using an Olympus microscope (40 \times and 60 \times magnification). The foams were studied during periods up to a few months.

3. Results and Discussion

3.1 Surface tension measurements

The time evolution of the surface tension γ for a fixed particle concentration (1wt.%) and different surfactant concentrations (always below the critical micellar concentration (CMC, $9.2 \times 10^{-4} \text{M}$)) is shown in Figure 1A.

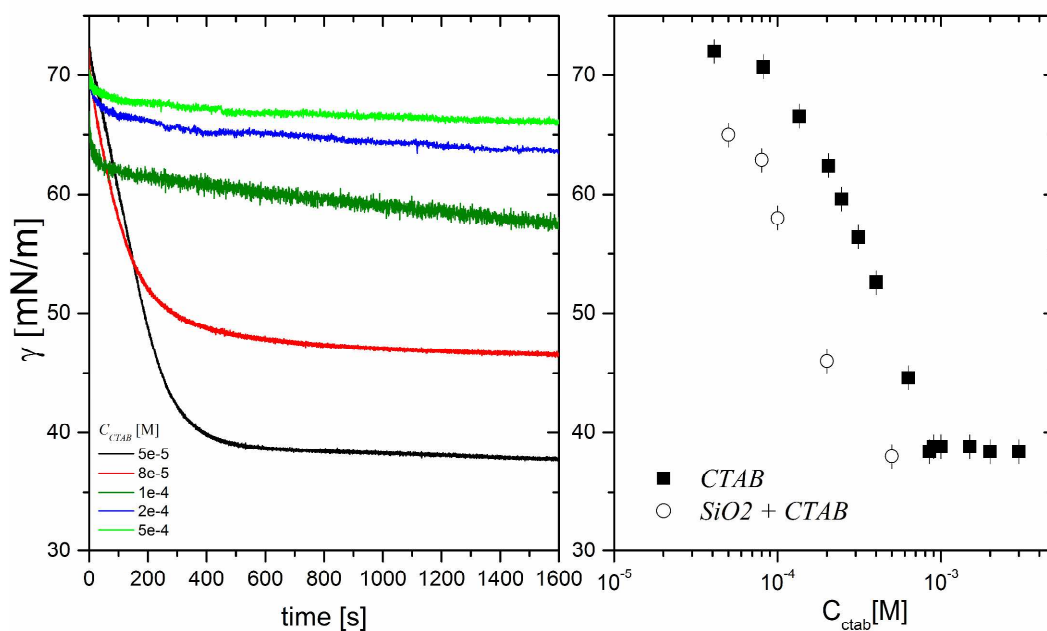


Fig. 1: Interfacial tension measurements. (A) Time variation of the surface tension γ of silica nanoparticles dispersions for different CTAB concentrations. (B) Equilibrium surface tension as a function of CTAB concentration, with and without particles. We recall that 1mM NaBr was present in all the samples.

After an initial rapid decrease, the surface tension continues to evolve slightly over long periods of time, possibly due to very slow rearrangements in the surface layers or slight contamination occurring during long measurement times³⁶. It could also be continued slow adsorption. However, the amplitude of this long time decrease is smaller than the reproducibility of the measurements ($\pm 1 \text{mN/m}$) and does not affect the determination of

the surface tension at long times. Figure 1B shows the surface tensions γ_0 obtained after $\sim 10^3$ s. We found that γ_0 decreases significantly with increasing surfactant concentration. It is noteworthy that in all the samples containing particles, the values of γ_0 are lower than in the solutions of the pure surfactant at the same concentration, due to synergistic effects –well documented in the literature.⁹

In all the following experiments, we wait for one hour before starting the experiment to be sure that the surface tension has reached its stationary value γ_0 .

3.2 Bubble compression

During foam coarsening the smallest bubbles shrink and the largest expand. In order to better understand this behaviour in our systems, we have studied the response of individual bubbles to compression. For this purpose, a bubble of volume ranging from 4 to 12 mL is created and left to equilibrate until the surface tension has reached its stationary value γ_0 . At this point the bubble is compressed at a volumetric rate of 0.5 mL/s, resulting in an initial area compression rate of 450 cm²/min. A sequence of images taken during the different deflation states of these nanoparticle-covered bubbles is shown in Figure 2B (time increases from right to left). The surface tension is measured throughout the compression.

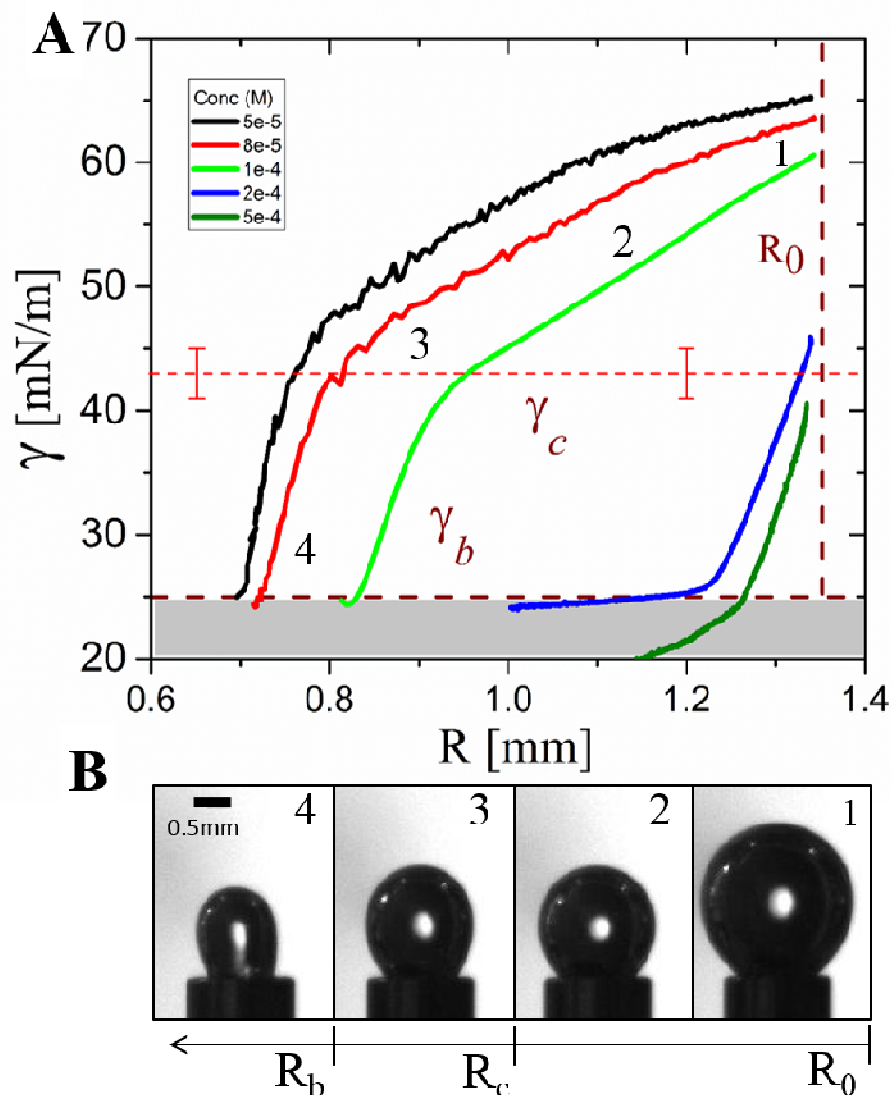


Fig. 2: *Forced compression of an air bubble immersed in an aqueous dispersion of CTAB-decorated SiO₂ nanoparticles (1wt.%).* (A) Interfacial tension γ as a function of the bubble radius R at different CTAB concentrations. In the region coloured in grey the bubbles are no longer Laplacian and the interfacial tension values are unreliable. (B) Sequence of images corresponding to the air bubble in the tensiometer during the compression experiment (time increases from right to left).

Figure 2A shows the dependence of the surface tension γ on the bubble radius R for CTAB-decorated silica nanoparticle layers covering the air bubble with different surfactant concentrations, ranging from 5×10^{-5} to 5×10^{-4} M. In all the experiments

performed, the bubbles start shrinking from the same initial radius R_0 (1.35mm), but have a different initial surface tension γ_0 , depending on the CTAB concentration studied (see Figure 1B).

Figure 2A shows that in all cases γ decreases with decreasing R , starting from the initial values γ_0 and R_0 , down to γ_c and R_c . Below $\gamma_c \approx 43 \pm 2$ mN/m, a change in the slope is observed. We identify this point as a jamming transition by analogy with previously published works^{25, 37} and following our observations made in a Langmuir trough (see supplementary material). If the CTAB concentration is high enough so that the equilibrium surface tension is already close to or below the critical surface tension γ_c , the surface tension curve starts directly in the second regime with the increased slope. This means that jamming can be achieved through two different routes. Through the compression of a loosely covered interface (CTAB $< 10^{-4}$ M), or directly through adsorption by making the particles more hydrophobic.

Upon further compression, beyond a radius R_b the bubble surface buckles, and is characterised by a non-Laplacian shape (Figure 2B, image 4). This occurs at another characteristic value of the surface tension $\gamma_b \approx 25$ mN/m, which also seems independent of the CTAB concentration. The non-Laplacian shape of the bubble means that the surface tension is no longer correctly measured. The data are still shown so that the transition in the slope can be observed. This shows a change in the response of the interface. In all the figures the surface tension measurements with a non-Laplacian bubble shape are shaded in grey and have to be taken carefully.

Compression studies were also performed on planar surfaces using a Langmuir trough. This allows us to confirm the values γ_c of the critical surface tension at the jamming transition and γ_b for the buckling transition (Figure S1A and S2) using the Wilhelmy

technique, rather than the drop shape analysis. Moreover, Brewster angle microscopy on the Langmuir layer provides information on the particle organisation (Figure S1B). For reasons of clarity, we present the details of those studies in the supplementary materials. While the critical surface tensions and the overall shape of the isothermal curves obtained by the Langmuir technique were similar to those obtained by the rising bubble technique, the quantitative values for γ (A) differed significantly between both techniques (Figure S2). The compression rates are different, between 100 - 1000 cm^2/min (depending on the bubble size) with bubbles, compared with 5 cm^2/min in the Langmuir trough. The differences might also be due to the different compression geometry: the uni-axial compression on a planar surface involves shear and compressional deformation, while the compression of the bubble surface is almost purely compressional. Indeed, the elastic moduli measured in the Langmuir trough are higher than those measured using the compressed bubble, as expected (the uniaxial compression modulus being the sum of the isotropic modulus E and of the shear modulus³⁸).

In conclusion, the measurements performed in Langmuir trough and in deflating bubbles are not quantitatively comparable. Nevertheless, the values of γ_c and γ_d are similar, which allows us to talk about “jamming” and “buckling” in the rising bubble experiment.

(i) Effect of changing the initial bubble volume

We have also investigated the effect of the initial bubble radius R_0 by varying the initial volume V_0 . Changing the initial bubble volume while keeping the volume compression rate constant (at 0.5 mL/s in this case) leads to an increase of the surface compression

rate dA/dt with decreasing bubble radius R since $dA/dt = (2/R) dV/dt$. The surface compression rate is plotted in the inset of Figure 3 (B), and can be seen to vary between around 100 - 1000 cm^2/min . The smaller the radius, the larger the surface compression rate, as expected. This means that we probe different compression rates using the different bubbles sizes.

We chose one CTAB concentration (2×10^{-4} M), sufficiently high to be in the jammed regime from the onset of the compression. As it can be seen in Figure 3A, the stationary surface tension γ_0 corresponding to the adsorption of the surfactant-decorated particles at the air/liquid interface is independent of the initial bubble radius R_0 . Once the shrinking process starts, the trend is similar in all cases leading to the same value of γ_b ($\approx 25 \text{mN/m}$) for the onset of the buckling transition.

In Figure 3B, we have re-scaled the experimental results corresponding to Figure 3A by plotting $\gamma - \gamma_0$ against R_0^2/R^2 . The latter corresponds to the inverse ratio of the surface area of the bubble to the initial surface area before compression; *i.e.* it corresponds to the change in surface concentration of the particles since they are assumed to be irreversibly adsorbed. The curves collapse reasonably, except for the smallest bubble, possibly due to larger measurement uncertainties in this case.

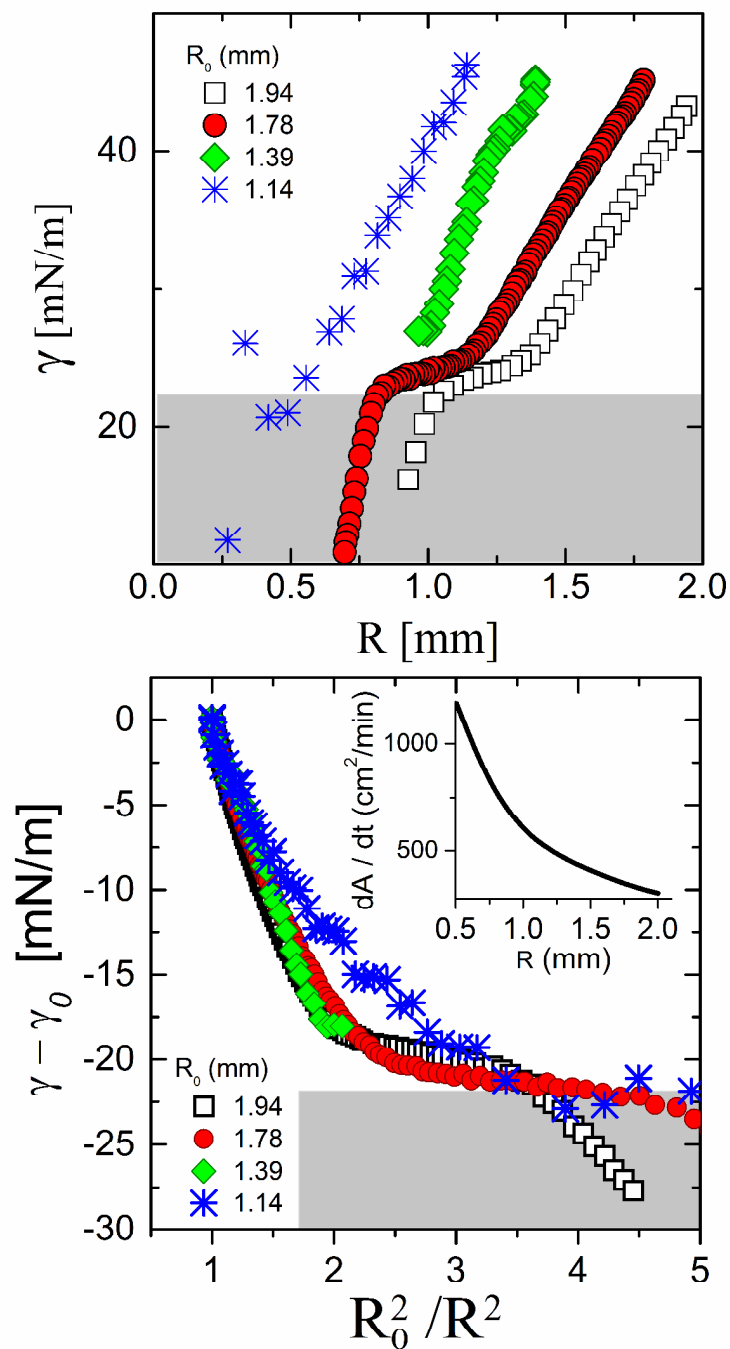


Fig. 3: (A) Sample with 2×10^{-4} M CTAB with bubbles of different initial volumes V_0 . The region where the bubble is no longer Laplacian is shaded in grey. (B) Change of surface tension of a bubble coated by CTAB-decorated nanoparticles versus the ratio R_0^2/R^2 , where R_0 corresponds to the initial radius of the bubble. Inset: Surface compression rates versus initial radius R .

Let us rationalise this scaling. From the definition of the surface compression modulus $E = A \, d\gamma/dA$, we obtain for spherical bubbles: $E = R^2 \, d\gamma/dR^2$. Assuming that E is relatively constant, this can be integrated into $\gamma = \gamma_0 - E \ln (R_0^2/R^2)$, which - for small R_0^2/R^2 - leads to:

$$\gamma - \gamma_0 \approx E \cdot \left(1 - \frac{R_0^2}{R^2}\right). \quad (2)$$

This means that a linear variation of the surface tension with the quantity R_0^2/R^2 corresponds to a constant value of elasticity E . In Figure 3B we can distinguish two separate zones. The three curves with $V_0 = 6, 10$ and $12 \, \mu\text{L}$ have collapsed into one. In the early stages of compression they form a straight line with a common and constant elastic modulus of $70 \, \text{mN/m}$. The collapse of the data means that the compression rate has almost no influence on the elasticity of the interface (in the range high surface compression rates explored here). Further compression of the surface gives rise to a distinct change of slope at the buckling transition, the slope becomes much smaller.

(ii) Effect of the CTAB concentration on surface elasticity.

Let us now go back to the situation where we fix the initial bubble size (i.e. the compression rate) while varying the CTAB concentrations. Figure 2 shows that the jamming and buckling transitions are reached after less compression if the surfactant concentration is larger. This is likely because the surface density at the beginning of the compression is larger as suggested by the lower γ_0 . It appears that the jamming transition occurs at a common value around $43 \pm 2 \, \text{mN/m}$. In the case of $2 \cdot 10^{-4} \, \text{M}$ and $5 \cdot 10^{-4} \, \text{M}$ CTAB, the entire bubble surface is already covered by particles before the start of compression since $\gamma_0 < \gamma_c$.

Since γ_b is rather independent of the surfactant concentration, we have re-plotted the data for the different surfactant concentrations as a function of R_b^2/R^2 in figure 4. All the different curves then collapse onto a master curve. This is surprising. It suggests that the surface concentrations leading to jamming and buckling are independent of the surfactant concentration.

This curve shows the three distinctive regimes discussed before, separated by a jamming transition at $\gamma = \gamma_c$ and a buckling transition at $\gamma = \gamma_b$. The two first regimes for $\gamma > \gamma_b$ are characterised by a linear dependence of γ with the ratio R_b^2/R^2 , but with a different slope. As in equation 2, we can expand γ as a function of R_b^2/R^2 around γ_b :

$$\gamma \approx \gamma_b + E \left(1 - \frac{R_b^2}{R^2} \right) \quad (3)$$

The linear dependence means that elasticity is constant for the different surfactant concentrations. It suggests that the mechanical properties of the interface do not depend on the surfactant concentration, which controls the particle hydrophobicity and the particle-particle interactions. This is unexpected and further suggests that what controls this is simply the particle surface coverage. For $\gamma > \gamma_c$, $E = 10$ mN/m and is less than $\gamma_c / 2$ (Gibbs criteria is not fulfilled). For $\gamma_c < \gamma < \gamma_b$, $E = 70$ mN/m and is larger than $\gamma_c / 2$ (Gibbs criteria is fulfilled). Therefore one of the criteria for the arrest of coarsening of bubbles is fulfilled once the interfaces are jammed.

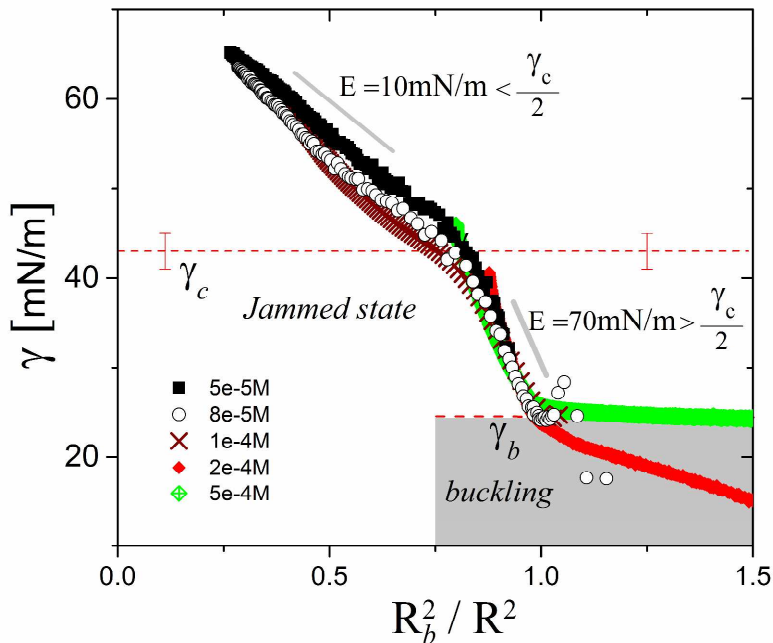


Fig. 4: Surface tension of a bubble coated by CTAB-decorated nanoparticles for different CTAB concentrations versus the ratio R_b^2/R^2 , where R_b corresponds to the radius at which the particle layers start to buckle at the surface of the bubble. The value of γ_c and γ_b are very similar in all the cases considered. The grey region corresponds to the buckled state in which the bubbles have non-Laplacian shapes. $R_0 = 1.35$ mm.

(iii) *Pressure analysis*

Let us now correlate the values obtained for the compression elastic modulus to the Gibbs stability condition^{16, 17, 39}. Gibbs considered a unique isolated bubble which spontaneously dissolves due to the difference in Laplace pressure with the surrounding media ($\Delta P = P_{in} - P_{ext} = 2\gamma/R$). Without the presence of compression elasticity, the change in bubble pressure due to a change in bubble radius $d\Delta P/dR$ is always negative

$$\frac{d\Delta P}{dR} = \frac{-2\gamma}{R^2} < 0, \quad (4)$$

leading to an unstable situation and an increasingly rapid dissolution of the bubble. This destabilisation may be counteracted by the presence of a compression modulus E (Eq. 1) such that

$$\frac{d\Delta P}{dR} = \frac{-2\gamma}{R^2} + \frac{4E}{R^2} > 0. \quad (5)$$

If $E > \gamma/2$, $d\Delta P/dR > 0$ and thus the bubble pressure decreases as its radius decreases, and the bubble dissolution slows down until it is stable against dissolution when $\Delta P = 0$. Since $\Delta P = 0$ implies a zero-mean curvature of the bubble surface, the bubble necessarily has to accommodate opposite curvatures within its surface, which leads to a faceted or a buckled shape once this point is reached.

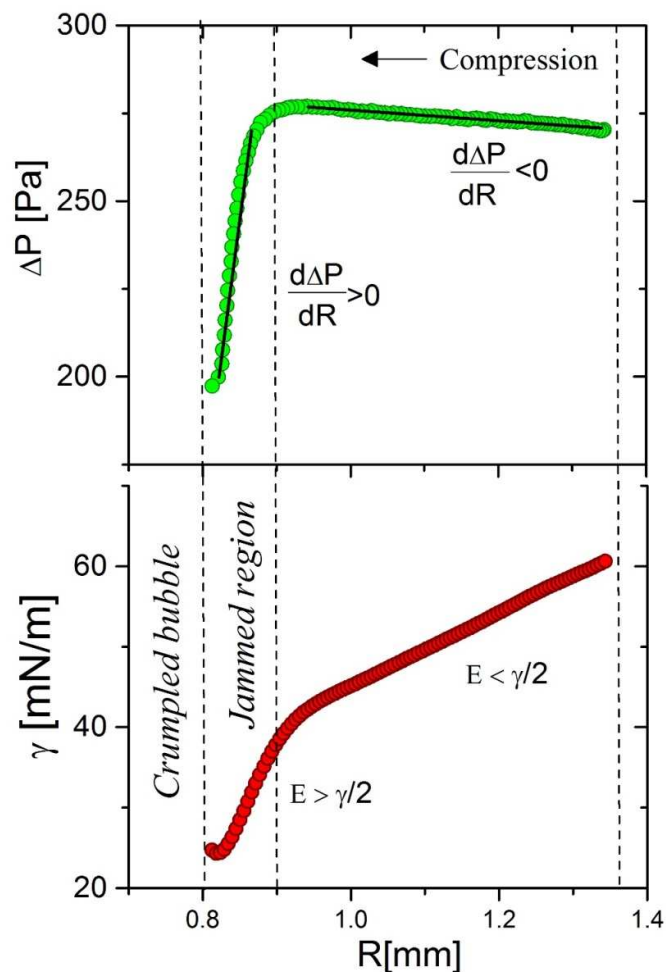


Fig. 5: (Top) Bubble pressure ΔP and (Bottom) surface tension γ versus the radius of a bubble coated by CTAB-decorated SiO_2 nanoparticles (10^{-4} M CTAB).

We measured the bubble pressure during the shrinkage process of bubbles in particle/surfactant dispersions. Figure 5 shows the bubble pressure versus the bubble radius for 10^{-4} M CTAB. For $\gamma > \gamma_c$, $d\Delta P/dR < 0$, in agreement with the fact that $E < \gamma/2$. In turn, below γ_c , $d\Delta P/dR > 0$, in agreement with the fact that $E > \gamma/2$. This result suggests that foam coarsening could be stopped once the particles jam at the bubble surface once the bubbles have shrunk sufficiently. The criteria $E > \gamma/2$ is necessary to stop coarsening but certainly not sufficient. Indeed, in addition, the jammed surface

must resist collapse. That is why most protein foams coarsen even if the surface elastic moduli are larger than $\gamma/2$. During bubble shrinkage, the surface concentration increases and these proteins start forming multilayers with almost no elastic resistance¹⁵. We will see in the next section that this is not the case in our experiments.

3.3 Foam studies

Up to now we discussed the response of single interfaces and isolated bubbles coated by CTAB-decorated colloids to compression. In this section, we will discuss how the particles can increase the resistance of foams against coarsening. Figure 6 shows the results of foam stability tests for all the dispersions investigated. The foams were generated by hand-shaking.

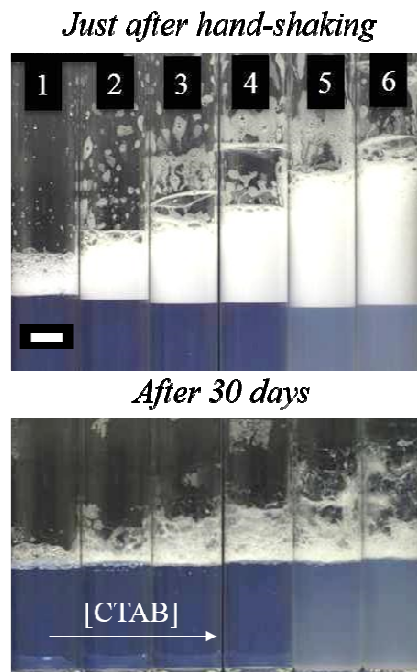


Fig. 6: A sequence of images showing the long-term evolution of foams created by CTAB-covered silica nanoparticles as a function of the CTAB concentration. CTAB

concentration: **1:** $5 \cdot 10^{-5} \text{M}$; **2:** $5 \cdot 10^{-5} \text{M}$, **3:** $8 \cdot 10^{-5} \text{M}$; **4:** 10^{-4}M ; **5:** $2 \cdot 10^{-4} \text{M}$; and **6:** $5 \cdot 10^{-4} \text{M}$. The scale bar length is 10mm.

In the top of Fig. 6 one can see that the foaming capacity increases with increasing surfactant concentration, but the long time stability is similar for all the foams. We observe two regimes. During the first month, the foam ages and both coarsening and coalescence are observed (Figure 6). One month after foam generation, a small quantity of bubbles remains at the bottom close to the bulk dispersion. These remaining bubbles are very stable (Figure 7A). Once they reach their final size, they keep their size and shape. Even the remaining millimetric bubbles observed in Figure 7A are unchanged during the following ten days. A sequence of pictures obtained at different magnifications shows that these bubbles are “crumpled”, i.e. they have buckled surfaces (Figure 7 B and C). The interfaces buckle, and do not collapse (as also confirmed by the BAM images (Figure S1). The interfacial resistance combined with the fulfillment of the Gibbs criteria arrests coarsening.

From our observations on individual bubbles we therefore propose the following scenario for the foam coarsening: in the first stage, the surface concentration of particles is small so the surface tension value stays larger than γ_c . The surface elasticity is then smaller than $\gamma/2$, $d\Delta P/dR < 0$ and the bubbles coarsen, as expected. The foam ageing leads to an increase of the concentration of particles at the interface of the shrinking bubbles as the particles cannot desorb from the interface. The shrinkage proceeds until $d\Delta P/dR > 0$, which is the case when $\gamma < \gamma_c$. As γ_c is reached, the surface concentration of particles is sufficiently high so that they are in a jammed state. Coarsening slows down dramatically beyond this point and should stop when $\Delta P=0$. In samples where the

concentration of CTAB is sufficiently, the interfaces are almost immediately jammed and the coarsening proceeds slowly until $\Delta P=0$.

The quantitative comparison of single bubble experiments with a foam should be made with caution, for several reasons. The scenario explained above allows understanding qualitatively the behaviour of the shrinking bubbles but what prevents the larger ones to grow is rather unclear. The interfacial compression is done at rates very different from that of coarsening bubbles, which can be cm^2 in hours or days rather than minutes. For a collection of bubbles –a foam– ΔP is the pressure difference between two neighbouring bubbles, and it cannot be related in a straightforward way to the pressure inside an isolated bubble. This is due to the fact that in foams ΔP depends on the bubble geometry¹ and on the surface tensions of the bubbles (when working with irreversibly adsorbed systems, the surface tension of adjacent bubbles can be different).

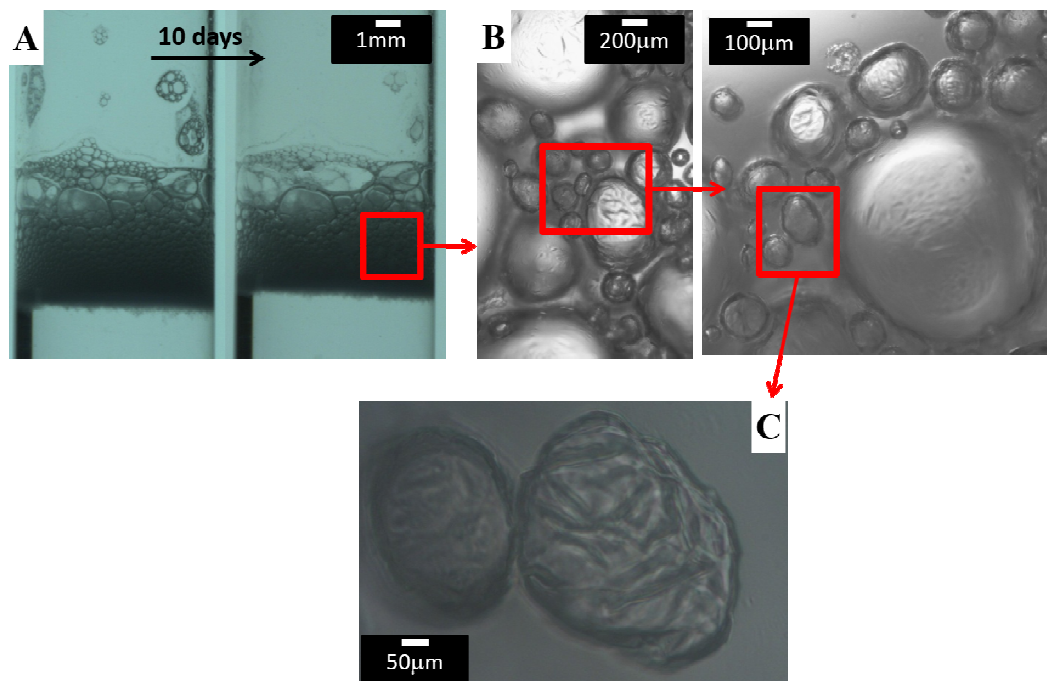


Fig. 7: From macro- to microscale. (A) Set of two images showing the long-term evolution of a foam stabilised by surfactant-particle dispersions, after 30 days and 40 days (SiO_2 : 1wt.% and CTAB: 2×10^{-4} M). (B) Optical micrograph of a set of crumpled bubbles that remain stable during the ten days. (C) Optical micrograph showing in detail two crumpled bubbles due to the buckling of the particle laden interface.

4. Conclusion

We have used surfactant-decorated nanoparticles to investigate the shrinkage behaviour of isolated bubbles and of bubbles contained in foams. Our observations show that the compression of the irreversibly adsorbed particle layers at the surface of the bubbles leads to three distinct regimes which are independent of the initial bubble size and, more surprisingly, of the surfactant concentration:

1. $\gamma < \gamma_c$: Below a critical surface tension γ_c the surface tension decreases linearly with decreasing bubble surface, leading to a well-defined compression elasticity of $E \approx 10$ mN/m. Here $E < \gamma/2$, hence the bubble pressure increases with decreasing bubble size.
2. $\gamma_c < \gamma < \gamma_b$: Beyond a critical surface tension γ_c and above γ_b the particles seem to jam in the bubble surface, leading to a solid-like surface behaviour. The surface tension decreases more dramatically (yet still linearly) with decreasing bubble surface, leading to a well-defined compression elasticity of $E \approx 70$ mN/m. Here $E > \gamma/2$, hence the bubble pressure decreases with decreasing bubble size, leading to a slowing down of spontaneous bubble dissolution.

3. $\gamma < \gamma_b$: Beyond a second critical surface tension γ_b , the bubble surface buckles, leading to indefinitely stable bubbles. The surface tension and surface elasticity of these bubbles could not be measured with our techniques.

The observations are in line with experiments made in the Langmuir trough [SI] and with experiments with oil drops stabilised with particles only¹⁸. In this study, the onset of buckling is associated to the moment where the internal pressure in the bubble vanishes, hence when the Gibbs criteria is reached.

The microscopic interpretation of our results is not obvious. But we can infer that at the jamming transition the particles start to strongly interact with each other, leading to the increase in E . The packing increases until the buckling transition where they cannot compact any further, so the surface starts to buckle.

What is noticeable is that the surface tensions at which we observe both transitions do not depend on the surfactant concentration although the initial surface tension does. The interface behaves as a simple surfactant system at thermodynamic equilibrium, so with a unique equation of state (link between surface tension and surface concentration of particles). A picture of this would be the following: the surfactant concentration has an influence on the initial coverage in decorated nanoparticles, leading to a different surface tension. But the behaviour under compression only depends on the particle coverage so a simple rescaling leads to a collapse of the data. This scenario is also backed up by the constant surface elasticity in the different regimes, independent of the surfactant concentration.

Although the compression “*isotherms*” with CTAB coated particles are independent of surfactant concentration, they are surely different if the surfactant is changed. It is already known that the same particles functionalised using shorter chain length

surfactants (*e.g.*, amines²⁸) do not arrest coarsening and that the foams they stabilise disappear. However, silica particles hydrophobised using double chained surfactants results in the arrest of coarsening at an even earlier stage²⁷. The differences arise due to the differences in the surfactant chain length, which when sufficiently long can promote attractive interactions between the particles –namely hydrophobic forces, which could also change the contact angle at the interface.

While the coarsening behaviour of an individual bubble is reasonably straightforward to analyse, the collective coarsening process of bubbles within a foam is much more complex. Only some bubbles shrink, while others grow and the pressure difference which drives the coarsening depends on the shape and surface tension of both neighbouring bubbles. The surface of the growing bubbles is seemingly never sufficiently well covered and further expansion of these bubbles can never be arrested. They coalesce with other large bubbles and finally with the surrounding air, leading to their complete disappearance. This is why only small bubbles remain at the end of the aging process. Those bubbles may be considered as isolated bubbles and are very stable because (i) the Gibbs criterion is fulfilled and (ii) the interface is strong enough to resist collapse. If this second condition is not fulfilled, the foam would continue to coarsen until completely disappeared²⁸. This leads to a two-step scenario where (i) the foam coarsens with big bubbles growing continuously until rupture and (ii) the remaining small bubbles reach the Gibbs criteria and stop coarsening.

The coarsening in a collection of polydisperse bubbles is thus a complex process. However, controlled experiments at the bubble scale allow for qualitative predictions to the arrest of the coarsening through interfacial jamming and buckling. This result could in principle be generalised to emulsions. It is generally claimed that particle stabilised emulsions are stable because the drop surfaces are covered by a solid layer of jammed

nanoparticles⁴⁰. This is a criteria close to but not equivalent to the one we give in this article. Long term stability indeed involves the arrest of coarsening, which can hardly be achieved by a thin layer, even solid, if its compression modulus is not high enough. Indeed, an emulsion stabilised by solid interfacial layers will be stable against coarsening only when the radius of the drops is in the order of the thickness of the surface layer¹⁵. Indeed, Erni et al²⁰ observed that coarsening can be arrested in emulsions stabilised with polymers, if the layer becomes solid like. In their paper, the Gibbs criteria was not discussed but it was fulfilled. The description that we propose for foams should then be valid for emulsions as well.

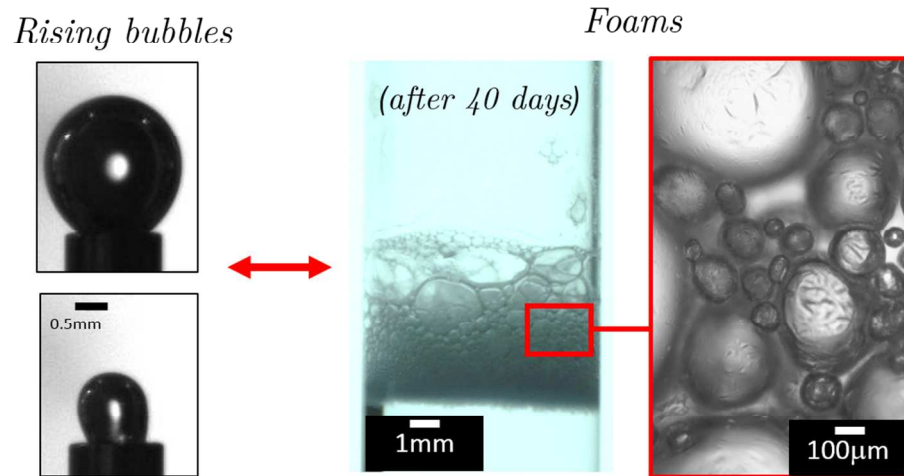
Acknowledgements

This work was supported in part by the CNRS (postdoctoral fellowship of A. Maestro), by the French space agency (CNES) and the European space agency (ESA). We acknowledge funding from the European Union (ERC POMCAPS).

References:

1. Weaire, D.; Hutzler, S., *The Physics of Foams*. Clarendon Press: Oxford, 1999.
2. Prud'homme, R. K.; Khan, S. A., *Foams: Theory, Measurements, and Applications*. Marcel Dekker: 1996.
3. Langevin, D. *Chemphyschem* **2008**, 9, (4), 510-522.
4. Du, Z.; Bilbao-Montoya, M.; Binks, B.; Dickinson, E.; Ettelaie, E.; Murray, B. *Langmuir* **2003**, 19.
5. Dickinson, E. *Langmuir* **2004**, 20, 8517-8525.
6. Kostakis, T.; Ettelaie, R.; Murray, B. *Langmuir* **2006**, 22, 1273-1280.
7. Binks, B. P.; Horozov, T. S. *Angewandte Chemie International Edition* **2005**, 44, (24), 3722-3725.
8. Cervantes Martinez, A.; Rio, E.; Delon, G.; Saint-Jalmes, A.; Langevin, D.; Binks, B. P. *Soft Matter* **2008**, 4, (7), 1531-1535.
9. Gonzenbach, U. T.; Studart, A. R.; Tervoort, E.; Gauckler, L. J. *Angewandte Chemie-International Edition* **2006**, 45, (21), 3526-3530.
10. Hunter, T. N. *Advances in Colloid and Interface Science* **2008**, 137, 57-81.
11. Tang, F. Q. *Journal of Colloid and Interface Science* **1989**, 131, 498-502.
12. Fujii, S. *Langmuir* **2006**, 22, 7512-7520.
13. Alargova, R. G.; Warhadpande, D. S.; Paunov, V. N.; Velev, O. *Langmuir* **2004**, 20, 10371-10374.
14. Abkarian, M.; Subramaniam, A. B.; Kim, S.-H.; Larsen, R. J.; Yang, S.-M.; Stone, H. A. *Physical Review Letters* **2007**, 99, (18), 188301.
15. Meinders, M. B. J.; van Vliet, T. *Advances in Colloid and Interface Science* **2004**, 108, 119-126.
16. Gibbs, J. W., *The Collected works*. Longmans, Green and co.: 1928; Vol. 1.
17. Blijdenstein, T. B. J.; de Groot, P. W. N.; Stoyanov, S. D. *Soft Matter* **2010**, 6, (8), 1799-1808.
18. Monteux, C.; Kirkwood, J.; Xu, H.; Jung, E.; Fuller, G. G. *Physical Chemistry Chemical Physics* **2007**, 9, (48), 6344-6350.
19. Datta, S. S.; Shum, H. C.; Weitz, D. A. *Langmuir* 26, (24), 18612-18616.
20. Erni, P.; Huda, A. J.; Wonga, K.; Parker, A. W. *Soft Matter* **2012**, 8, 6958-6967.
21. Zang, D. Y.; Rio, E.; Langevin, D.; Wei, B.; Binks, B. P. *European Physical Journal E* **2010**, 31, (2), 125-134.
22. Bormashenko, E.; Musin, A.; Whyman, G.; Barkay, Z.; Starostin, A.; Valtsifer, V.; Strelnikov, V. *colloids and Surfaces a-Physicochemical and Engineering Aspects* **2013**, 425, 15-23.
23. Erni, P. *Soft Matter* **2011**, 7, (17), 7586-7600.
24. Garbin, V.; Crocker, J. C.; Stebe, J. K. *Langmuir* **2011**, 28, 1663-1667.
25. Binks, B. P. *Curr. Opin. Colloid Interface Sci.* **2002**, 7, 21-41.
26. Gonzenbach, U. T.; Studart, A. R.; Tervoort, E.; Gauckler, L. J. *Angewandte Chemie International Edition* **2006**, 45, (21), 3526-3530.
27. Binks, B. P.; Kirkland, M.; Rodrigues, J. A. *Soft Matter* **2008**, 4, (12), 2373-2382.
28. Arriaga, L. R.; Drenckhan, W.; Salonen, A.; Rodrigues, J. A.; Iniguez-Palomares, R.; Rio, E.; Langevin, D. *Soft Matter* **2012**, 8, (43), 11085-11097.
29. Ravera, F.; Santini, E.; Loglio, G.; Ferrari, M.; Liggieri, L. *The Journal of Physical Chemistry B* **2006**, 110, (39), 19543-19551.

30. Maestro, A.; Guzman, E.; Santini, E.; Ravera, F.; Liggieri, L.; Ortega, F.; Rubio, R. G. *Soft Matter* **2012**, *8*, 837-43.
31. Santini, E.; Krägel, J.; Ravera, F.; Liggieri, L.; Miller, R. *Colloids and Surfaces A: Physicochemical and Engineering Aspects* **2011**, *382*, (1-3), 186-191.
32. Anton, N.; Pierrat, P.; Lebeau, L.; Vandamme, T.; Bouriat, P. *Soft Matter* **2013**, *9*, 10081-10091.
33. Loglio, G.; Pandolfini, P.; Miller, R.; Makievski, A. V.; Ravera, F.; Ferrari, M.; Liggieri, L., *Drop and bubble shape analysis as a tool for dilational rheological studies of interfacial layers*. 2001; Vol. 11, p 439-483.
34. Ravera, F.; Santini, E.; Loglio, G.; Ferrari, M.; Liggieri, L. *Journal of Physical Chemistry B* **2006**, *110*, (39), 19543-19551.
35. del Rio, O. I.; W., N. A. *Journal of Colloid and Interface Science* **1997**, *196*, 1366147.
36. Yazhgur, P. A.; Noskov, B. A.; Liggieri, L.; Lin, S. Y.; Loglio, G.; Miller, R.; Ravera, F. *Soft Matter* **2013**, *9*, 3305-3314.
37. Aveyard, R.; Clint, J. H.; Nees, D.; paunov, V. N. *Langmuir* **2000**, *16*, 1969-1979.
38. Petkov, J. T.; Gurkov, T. D.; Campbell, B. E.; Borwankar, R. P. *Langmuir* **2000**, *16*, 3703.
39. Stocco, A.; Drenckhan, W.; Rio, E.; Langevin, D.; Binks, B. P. *Soft Matter* **2009**, *5*, (11), 2215-2222.
40. Cui, M.; Emrick, T.; Russell, T. P. *Nature* **2013**, *342*, 460-463
41. Oettel, M.; Dietrich, S. *Langmuir* **2008**, *24*, (4), 1425-1441.
42. Yeung, A.; Zhang, L. C. *Langmuir* **2006**, *22*, (2), 693-701.



Interfacial jamming and buckling of particle-coated bubbles can result in the arrest of foam coarsening.

197x110mm (150 x 150 DPI)